A Study of Dust Structure around AGB Star in 60 and 100 µm IRAS Survey at Latitude 54.68°

Arjun Kumar Gautam and Binil Aryal

Journal of Nepal Physical Society

Volume 4, Issue 1, February 2017

ISSN: 2392-473X

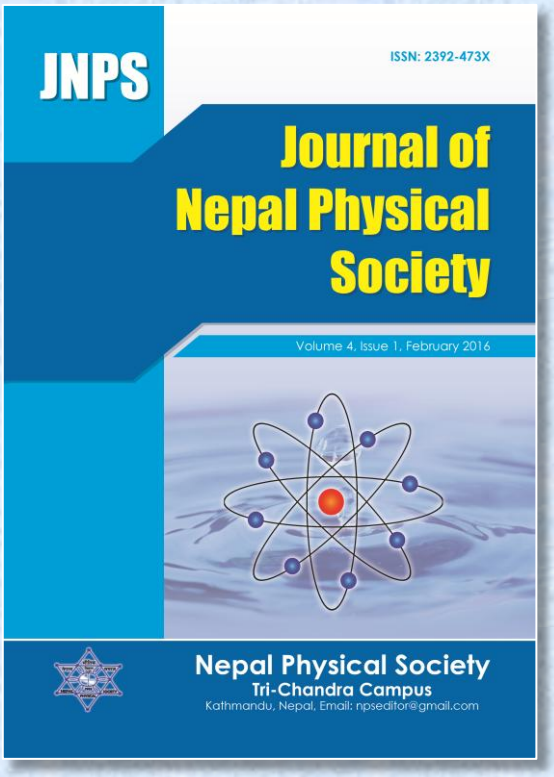

JNPS, **4** (1), 67-77 (2017)

Published by:

Nepal Physical Society

P.O. Box : 2934

Tri-Chandra Campus

Kathmandu, Nepal

Email: npseditor@gmail.com

JNPS ***4*** *(1), 67-77 (2017)*
ISSN: 2392-473X

Research Article

A Study of Dust Structure around AGB Star in 60 and 100 µm IRAS Survey at Latitude 54.68º

Arjun Kumar Gautam[1], and Binil Aryal[2, *]
[1]*Department of Physics, Bhaktapur Multiple Campus, Bhaktapur, Nepal*
[2]*Central Department of Physics, Tribhuvan University, Kirtipur, Nepal*
[*]*Corrosponding Email: baryal@gmail.com*

ABSTRACT

We have studied about the evolution of Asymptotic Giant Branch (AGB) stars, mass losses from them and a systematic search of AGB stars in J2000 coordinate system provided by K. W. Shu & Y. J. Kwon (2011) of dust structure in the far infrared range (100 µm and 60 µm). For dust structure IRAS survey was performed using Sky View virtual Observatory. The FITS images downloaded from sky view was processed using software Aladin v 2.5. A cavity like structure (major diameter∼1.93 pc & minor diameter∼ 0.89 pc) lies in the coordinate of R. A. (J2000) 04h 15m 03s and DEC (J2000) 54d 41m 00s was found at the distance∼ 240 pc. We studied the flux density variation and the temperature variation about major diameter, minor diameter and the distance between minimum temperature and minimum flux within the structure. We observed the variation of the temperature is 20.53 K to 21.09 K, with the offset of about 0.56 K, which show the cavity is independently evolved. The mass profile of each pixel of the structure was also calculated using this temperature.

Keywords: AGB Stars, Low and intermediate mass stars, Dredge-up, Thermal pulse, Nucleosynthesis, S-process, Mass loss, Excess mass.

INTRODUCTION

Low-to-intermediate mass stars end their life on the asymptotic giant branch (AGB) star. AGB stars are the main distributors of dust into the interstellar medium due to their high mass loss rates in combination with an effective dust condensation. It is therefore important to understand the dust formation process and sequence in their extended atmosphere. The interaction between wind and its surroundings in the interstellar medium (ISM) provides a laboratory to study the behavior of dust particles. Actually Asymptotic Giant Branch (AGB) stars are the final evolution stage of low- and intermediate-mass stars driven by nuclear burning. This phase of evolution is characterized by nuclear burning of hydrogen and helium in thin shells on top of the electron-degenerate core of carbon and oxygen, or for the most massive super AGB stars a core of oxygen, neon, and magnesium. In particular, the recurrent thermonuclear flashes that induce a complex series of convective mixing events provide a rich environment for nuclear production. The nucleosynthesis in AGB stars plays an important role for our understanding of the origin of the elements. AGB stars are the major contributors to the integral luminosity of intermediate-age stellar systems.

The spectra of AGB stars fall into very characteristic groups: the oxygen-rich stars, with spectra dominated by oxygen-containing molecules such as TiO, carbon-rich stars with spectra dominated by molecules containing carbon (e.g. CN, C_2), and rarer stars in between with C/O ≈ 1 (S stars). Examples of these spectra are shown in figure 1. The existence of these stars indicates that the products of helium burning in the interior of the star are being brought to the stellar surface. Any theory of AGB evolution must be able to explain this. While changes due to nuclear processes in the stellar interior occur on timescales of $\sim 10^5$ years, the outer envelopes of AGB stars pulsate on timescales of ∼10-1000 days. The pulsations are first seen with very small amplitude and short period at low luminosities. The pulsations grow in amplitude with increasing luminosity up to amplitudes in bolometric magnitude of ∼1 mag. and periods typically of 500- 1000 days. This large amplitude pulsation has a major consequence - it causes a very large increase in the mass loss rate, so that essentially

the entire envelope outside the nuclear burning core is lost. The star then evolves from the AGB through the post-AGB phase to the planetary nebula phase and ultimately to the white dwarf stage. During the planetary nebular phase, the envelope material lost in the AGB stellar wind is illuminated by energetic photons from the remnant star, thus creating the glowing planetary nebula.

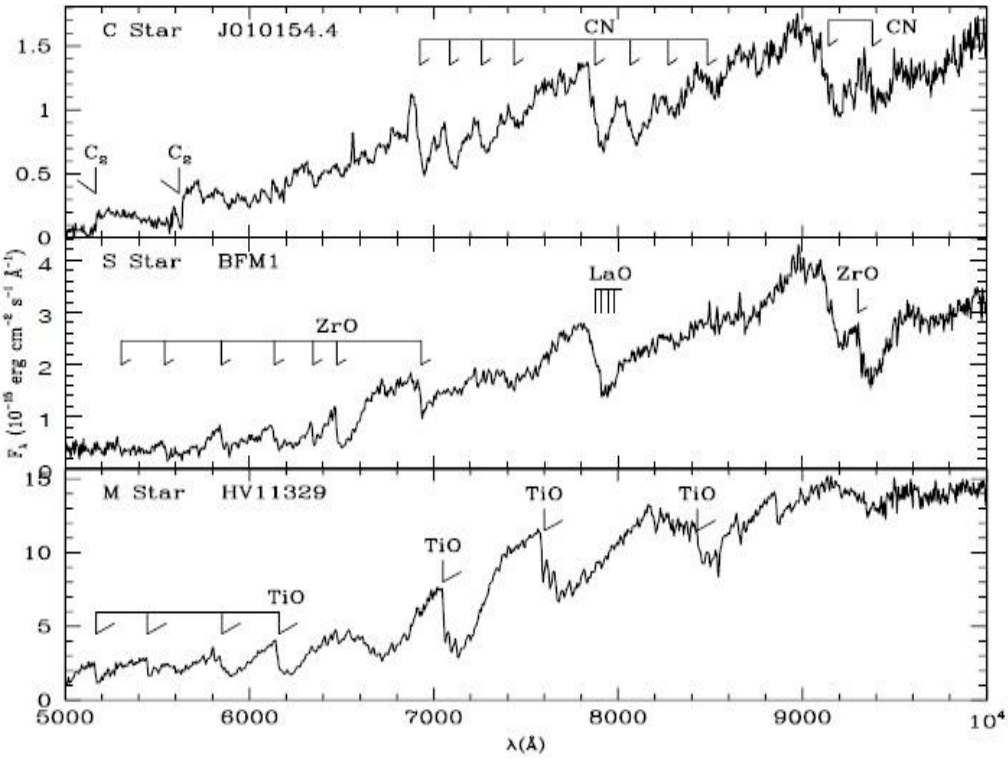

Fig.1. The distinctive spectra of an M star, an S star and a C star. The sequence M→S→C corresponds to a change from C/O < 1 to C/O ∼ 1 to C/O > 1. M stars have spectra dominated by molecules containing oxygen (e.g. TiO, VO) while C star spectra are dominated by molecules containing carbon (e.g. CN, C_2). Some of the stronger bands are marked on the figure {source: P. R.Wood, SAIt 81,883 (2010)}.

In the remainder of this article, we will discuss the interior nuclear evolution of AGB stars, mass loss from them, estimation of dust color temperature, dust mass, excess mass, etc.

THE EVOLUTION OF AGB STARS

AGB stars have large, low density convective envelopes of radius several hundred R_{sun} surrounding a dense, electron-degenerate core of carbon and oxygen. Between the envelope and the core are hydrogen and helium burning shells, whose typical energy production can be seen as a function of time in figure 2. In the early AGB phase, following exhaustion of helium in the core, the H and He shells burn smoothly, but the He shell soon becomes unstable and starts a series of thermal relaxation cycles. The He burning shell is effectively dormant for about 80% of the time, but at the end of each dormant period, it ignites furiously (but hydrostatically), reaching peak energy generation rates of $\sim 10^8$ L_{sun} in the more massive cores. After several hundred years, the helium shell drops back to burning at a rate roughly in equilibrium with the surface luminosity of the star, taking over from the H burning shell as the main energy source. Over the next ∼20% of the shell flash cycle, the He burning shell burning rate gradually declines, while the H burning shell rate increases to again become the dominant energy source, so that a new shell flash cycle begins.

The duration of a shell flash cycle, like most properties of the nuclear burning core, depends mostly on the core mass (Wood & Zarro, 1981; Boothroyd & Sackmann, 1988a). For a 1 M_{sun} AGB star with a typical core of mass ∼0.6 M_{sun} the cycle length is $\sim 10^5$ years, while for an AGB star of initial mass more than ∼ 5 M_{sun} and a core mass of 0.9 M_{sun}, the cycle length is $\sim 10^4$ years.

A very important aspect of AGB evolution is mass loss. The loss of essentially all the hydrogen-rich envelope is what terminates AGB evolution and leaves a compact remnant star that evolves through the parts of the HR diagram occupied by post-AGB stars, planetary nebular nuclei and white dwarfs (figure 1). Figure 2 shows the typical evolution of the mass loss rate and the mass in a 1 M_{sun} AGB star - many more examples are given in Vassiliadis & Wood (1993). It is particularly notable that mass tends to be ejected in multiple stages, which coincide with the brighter parts of the shell flash cycle when the H-burning shell is active. The mass loss process in AGB stars is discussed further in the next section of this paper.

The large energy release at a helium shell flash and its subsequent transport by convection leads to mixing processes that bring nuclear burning products, especially carbon and s-process elements, to the stellar surface: this process causes the transformation of AGB stars from oxygen-rich M stars to carbon stars with C/O > 1. The material ejected from AGB stars is a major source of enrichment of the interstellar medium in ^{12}C and heavy s-process elements.

A general overview of the mixing processes is shown in figure 3. When the He shell ignites and releases a large amount of energy, the resulting temperature gradient is sufficient to drive convective energy transport, creating the Inter shell Convective Zone. This zone carries the carbon produced by He burning outward, but not to the convective envelope, so that carbon is not directly mixed to the stellar surface. However, when the energy dumped into the He burning zone finally escapes from the core into the envelope, after the Intershell Convective Zone has disappeared, the envelope convection moves inward in mass and dredges up carbon rich material within the mass region previously occupied by the Intershell Convective Zone. This process is called the Third Dredge-Up and is the mechanism by which carbon stars are formed.

Another important nuclear process that occurs in AGB stars is s-process nucleosynthesis, wherein heavy elements are created by the addition of neutrons to relatively abundant nuclei, such as those in the Fe-peak. For the process to occur, a source of neutrons is required. These neutrons come from two sources in AGB stars: the reactions $^{12}C(p,\gamma)\ ^{13}N(\beta^+\nu)\ ^{13}C(\alpha,n)\ ^{16}O$ and $^{14}N(\alpha,\gamma)\ ^{18}F(\beta^+\nu)\ ^{18}O(\alpha,\gamma)\ ^{22}Ne(\alpha,n)\ ^{25}Mg$. The first set of reactions need to occur in a region with a restricted number of protons, so that the ^{13}C is not converted to ^{14}N by proton absorption as would be the case with the CNO cycle operating in a H-rich region. Furthermore, the temperature needs to be higher than that in the vicinity of the H-burning shell if the reaction $^{13}C(\alpha,n)\ ^{16}O$ is to occur. The first condition (low H abundance) occurs in the partial mixing region left at the bottom of the H-rich convective envelope by third dredgeup (the light grey region in figure 3). The details of the amount of mixing here are very uncertain, but some sort of semi-convection seems to be involved (Hollowell and Iben, 1988). Because of the uncertainties in current evolution models, most nucleosynthesis calculations treat the amount of mixing (size of the "convective pocket") as a free parameter. The second condition (sufficiently high temperatures) was found by Straniero, *et al.* (1995) to exist in the convective pocket between He shell flashes. Although the reaction rates are slow, there is sufficient time for the s-process to occur in this interval. At the next He shell flash, s-process elements so produced are engulfed by the new inter shell convection zone and then partially dredged-up to the stellar surface by the subsequent third dredge-up event. Other s-process elements remain in the convective pocket at the base of the third dredge-up zone, ready to be further enhanced with neutrons in the next inter-flash interval.

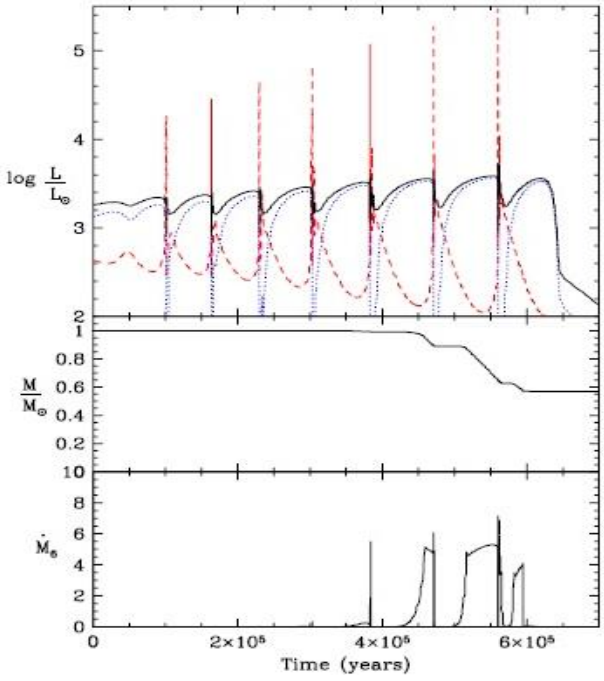

Fig. 2. The variation of L, LH (dotted line), LHe (dashed line), M and M˙ with time for a 1 M AGB star. This solar metallicity model is from the calculations of Vassiliadis & Wood (1993).

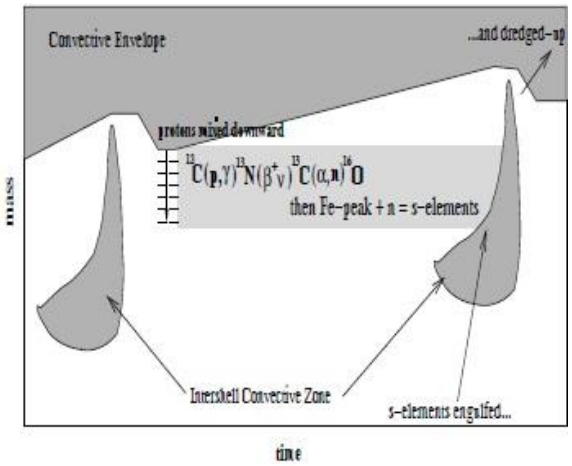

Fig. 3. A schematic diagram showing the positions of convection regions (dark grey) in the (mass fraction, time) plane. The light grey area is the region in which s-process nucleosynthesis occurs between He shell flashes. From Lattanzio & Wood (2004).

The second set of neutron-producing reactions also contribute to s-process nucleosynthesis. ^{14}N left over form the CNO cycle is readily burnt to ^{22}Ne soon after He burning shell ignition. However, the final reaction $^{22}Ne(\alpha,n)^{25}Mg$ requires temperatures near 3×10^{8} K, and is important mainly in the intershell convection zone of the more massive cores of the more massive AGB stars (Hollowell and Iben, 1988).

A consistent problem with all studies of mixing in AGB stars is our lack of knowledge of convective processes, especially the amount of overshoot occurring at the edges of convective regions. Convection is usually treated by the mixing length theory, and it is well known that the adopted mixing length significantly affects the amount of dredge-up (Wood, 1981; Boothroyd and Sackmann, 1988b; Lattanzio, 1989). Increasing the mixing-length enhances dredge-up. Attempts are now being been made to study mixing in AGB stars by using multi-dimensional fluid dynamics (Herwig *et al.*, 2006), rather than simple theories like the mixing-length theory. Much work remains to be done in this area.

The problems with numerical simulations of AGB stars has led to the creation of synthetic models of AGB evolution in which various aspects of the evolution, such as the amount of dredge-up at each helium shell flash and the minimum core mass at which dredge-up occurs, are treated as free parameters (Marigo and Girardi, 2007). The parameters of these models are then calibrated against observational data, such as the luminosities of carbon stars in the LMC (Large Magellanic Cloud) and SMC (Small Magellanic Cloud). The synthetic model calculations are useful when wide areas of parameter space (initial M and abundance) are to be explored.

MASS LOSS FROM AGB STARS

For a star to have a wind, there must be an outward force that provides momentum and energy input, accelerating the surface layers to velocities larger than the escape velocity. This may be realized in various ways, including the scattering of UV radiation by resonance line opacity in hot stars, the generation of magneto-acoustic waves above the photosphere in red giants, or the absorption of photons by dust grains in the outer atmospheres of the coolest and most luminous stars (Lamers and Cassinelli, 1999). Mass-loss dominates an AGB star's evolution and fate. It is clear from observations of Mira and OH/IR stars that mass-loss rates increase exponentially along the AGB until they reach super-wind values of $\sim 10^{-5} - 10^{-4}$ M_{sun} yr^{-1} (Willson, 2000; Olofsson, 2003).

Combining theoretical efforts and empirical evidence, a reasonable scenario takes form in which mass-loss on the AGB can be divided into three regimes: an initial period before the onset of the dust-driven wind (designated as "pre-dust mass-loss"); a subsequent phase characterised by an exponential increase of mass-loss driven by the combined action of dust and pulsation (designated as "dust-driven mass-loss"); and a final brief regime with high mass-loss (designated as "super-wind mass-loss").

In our scheme, the phase of pre-dust mass-loss (with rate $\dot{M}_{pre\text{-}dust}$) is thought to apply to the early stages on the AGB in which either dust has not yet formed in the outermost atmospheric layers, or if present in some small amount, is unable to generate an outflow. In these conditions a likely wind mechanism could be related to a strong flux of pressure waves or Alfven waves able to cause the spillover of the extended and highly turbulent chromospheres typical of red giants. The same mechanism might be at work during both the ascent along the RGB and the early stages of the AGB (Schroder and Cuntz, 2005; Cranmer and Saar, 2011).

In stellar evolutionary calculations a frequent choice to describe mass-loss during the early phases is the classical Reimers (1975) law, a simple

scaling relation of stellar parameters based on observations of few red giants and supergiants. The Reimers relation is commonly multiplied by an efficiency parameter η_R, whose value is calibrated such that it recovers the observed morphology of horizontal branch stars in Galactic Globular clusters. The calibration however, still depends on the residual envelope mass left over from the RGB (Renzini and Fusi Pecci, 1988).

More recently Schroder and Cuntz (2005) proposed a modified version of the Reimers (1975) law, in which additional dependencies on the effective temperature and surface gravity follow from a physically-motivated consideration of the mechanical flux responsible for the wind. The role of the chromosphere in driving mass-loss in lateK to early-M giants is supported by the analysis McDonald and van Loon, (2007) of the Hα and infrared calcium triplet lines in a sample of red giant stars hosted in Galactic globular clusters. Similarly to the Reimers relation, the Schroder and Cuntz (2005) formula also needs an efficiency parameter η_{SC} to be specified.

Novel efforts to model stellar winds from red giants were carried out by Cranmer and Saar (2011). A selfconsistent and more detailed theoretical approach is developed to follow the generation of energy flux due to magneto hydrodynamic turbulence from subsurface convection zones to its eventual dissipation and escape through the stellar wind. One major difference is that, while in Schroder & Cuntz (2005) the mass-loss rate is assumed to scale linearly with the photospheric mechanical energy flux (F_M) of Alfven waves ($\dot{M}_{pre\text{-}dust} \propto F_M$), the analysis of Cranmer and Saar (2011) yields a higher dependence ($\dot{M}_{pre\text{-}dust} \propto F_M^{12/7}$). Analytic models for magnetic wave generation indicate that the mechanical energy flux scales as $F_M \propto T_{eff}^{7.5}$ (Musielak and Rosner, 1988). Hence, considering that the mass-loss rate is proportional to the surface-integrated mechanical energy flux, $L_M = 4\pi R^2 F_M$, and expressing the stellar radius R with the Stefan-Boltzmann law for a black body, we eventually obtain a significantly steeper dependence of the mass-loss rate on the effective temperature,

$\dot{M}_{pre\text{-}dust} \propto T_{eff}^{3.5}$ (Schroder and Cuntz, 2005) and

$\dot{M}_{pre\text{-}dust} \propto T_{eff}^{8.86}$ (Cranmer and Saar,2011).

Following the pre-dust phase of mass-loss, as the star climbs the AGB at increasing luminosity, suitable conditions can be met in the cool atmosphere for stellar winds to be generated through a different intervening mechanism. The most plausible hypothesis resides in the momentum input when the stellar radiation field is absorbed (or scattered) by dust grains and transferred to the gas via collisions. This wind is enhanced by pulsations that shock the envelope and periodically levitate matter up to regions where dust can more efficiently condense (Gustafsson and Hofner, 2003). Observationally there is a clear correlation, though with a large scatter, between the mass-loss rate (here designated with $\dot{M}_{dust}$) and the pulsation period P of AGB variables, such that $\dot{M}_{dust}$ is seen to increase exponentially with the period (Vassiliadis and Wood, 1993).

Finally, close to tip of the TP-AGB, the mass-loss rates almost level out to $10^{-5} - 10^{-4} M_{sun}\ yr^{-1}$ of the so-called super-wind phase ($\dot{M}_{SW}$), corresponding to the condition in which the maximum momentum of the radiation field is transferred to the stellar atmosphere.

Within this framework, the mass-loss prescriptions adopted in the TP-AGB stellar models computed for this study are as follows. For the dust driven wind phase we adopt a formula similar to Bedijn (1988), which predicts an exponential increase of mass-loss $\dot{M}_{dust} \propto \exp(R^a M^b)$ dependent on stellar parameters derived from models of periodic shocked atmospheres. Coefficients a and b are calibrated on a sample of Galactic Mira stars (Marigo *et al.*, 2013; Nanni *et al.*, 2013, and Kalirai *et al*., 2014).

For the super-wind phase we adopt the formalism of Vassiliadis and Wood (1993), in which the mass-loss rate, $\dot{M}_{SW}$, is proportional to the ratio of the stellar luminosity to the terminal velocity of the gas, which itself scales linearly with the pulsation period. In practice as soon as $P > 500 - 600$ days the super-wind regime is expected to set in.

We keep the same prescriptions for $\dot{M}_{dust}$ and $\dot{M}_{SW}$ and vary only the $\dot{M}_{pre\text{-}dust}$. For the mass-loss rates $\dot{M}_{pre\text{-}dust}$ before the onset of dust-driven winds we consider four options:

- $\dot{M}^{\eta=0}_{\text{pre-dust}}$: no mass-loss before the possible onset of the dust-driven wind, $\dot{M}_{\text{pre-dust}} = 0$;
- $\dot{M}^{\text{R75}}_{\text{pre-dust}}$: the traditional Reimers (1975), mass-loss $\dot{M}_{\text{pre-dust}} = 4 \times 10^{-13} \eta_R$ L/ gR $= 4\text{x}10^{-13} \eta_R$LR/M with the efficiency parameter $\eta_R = 0.4$;
- $\dot{M}^{\text{SC05}}_{\text{pre-dust}}$: the original Schroder & Cuntz (2005) law $\dot{M}_{\text{pre-dust}} = 10^{-14}\ \eta_{SC}$ LR/ M $\left\{\frac{T_{\text{eff}}}{4000\text{K}}\right\}^{3.5} \left\{1 + \frac{1}{4300\ \text{g}}\right\}$ with the efficiency parameter $\eta_{SC} = 8.0$;
- $\dot{M}^{\text{MSC05}}_{\text{pre-dust}}$: a modified version of the Schroder & Cuntz (2005) scaling relation $\dot{M}_{\text{pre-dust}} = 10^{-12}\ \eta_{mSC}$ LR/ M $\left\{\frac{T_{\text{eff}}}{4000\text{K}}\right\}^{8.9} \left\{1 + \frac{1}{4300\ \text{g}}\right\}$

in which, for the reasons explained above, the power-law dependence on the effective temperature is steepened; here the efficiency parameter is set to $\eta_{mSC} = 0.4$.

In all formulas the mass-loss rate is given in M_{sun} yr^{-1}, the effective temperature T_{eff} is in Kelvin, the stellar radius R, luminosity L, the mass M, and surface gravity g are expressed in solar units.

Finally, we caution the reader that our modified Schroder and Cuntz relation, with $\eta_{mSC} = 0.4$, set for the early stages of the TP-AGB, may be too efficient to be extended to lower luminosities of RGB stars based on a quick comparison to the measured mass-loss rates of the sample, collected by Cranmer and Saar (2011), that includes metal poor RGB stars with and effective temperatures in the range 3800-5800 K, as a function of the luminosity.

DATA REDUCTION

Each pixels of the FITS image of our region of interest are analyzed using software Aladin v2.5 which is one of the handy and extensively used software in the data reduction processes. This software is designed to reduce and analyze the data collected from the ground based and space telescopes covering all wavelength regions. Information regarding the energy spectrum, relative flux density with coordinate of each pixel, different types of contour maps, longitude and the latitude of the desired structure can be obtained by using software .5 Contour Map.

We intend to study the isolated cavity structure at 60 μm and 100 μm. We adopt the method of drawing contours at different levels so that we can separate the region of maximum and minimum flux density. The best contour level of the selected FITS image is chosen in between 1 to 38.

We are interested in these maxima to study the flux density within the region because our focus is on the temperature profile and the mass distribution of the dust within the isolated structure. We are interested to study the temperature and mass profile of isolated structure and possibility of star formation in this region. The contour picture is shown in figure1.

FLUX DENSITY VARIATION

To calculate temperature and mass of each pixel due to the contribution of dust, we need flux density of all pixel lying inside the outermost contour i.e. isoconter level 40 at 60 μm and 100 μm respectively. It is done by using Aladin v2.5 to evaluate Variation of flux density with distance along major diameter (AB), minor diameter CD and the distance between minimum temperature and minimum flux density (EF).

DUST COLOR TEMPERATURE ESTIMATION

Adopting the similar method as that of Schnee *et al.* (2005) the dust temperature was calculated from the IRAS 60 μm and 100 μm flux densities (Dupac, 2003). By knowing the ratio of flux densities at 60 μm and 100 μm, the temperature contribution due to dust color can be calculated. The dust temperature T_d in each pixel of a FIR image can be obtained by assuming that the dust in a single beam is isothermal and that the observed ratio of 60 μm to 100 μm emission is due to black body radiation from dust grains at T_d, modified by a power law of spectral emissivity index. The flux density of emission at a wavelength λ_i is given by

$$F_i = \left[\frac{2hc}{\lambda_i^3\left(e^{\frac{hc}{\lambda_i kT_d}}\right) - 1}\right] N_d\, \alpha\, \lambda_i^{-\beta}\, \Omega_i \qquad (1)$$

where β is the spectral emissivity index, N_d is the column density of dust grains, α is a constant which relates the flux with the optical depth of the dust, and Ω_i is the solid angle subtended at λ_i by the detector. We use the equation following Dupac *et al.* (2003).

$$\beta = \frac{1}{\delta + wT_d} \quad (2)$$

to describe the observed inverse relationship between temperature and emissivity spectral index.

With the assumptions that the dust emission is optically thin at 60 μm and 100 μm and that Ωω∼ Ω100 (true for IRAS image), we can write the ratio, R, of the flux densities at 60 μm and 100 μm as

$$R = 0.6^{-(3+\beta)} \quad \frac{e^{144/T_d} - 1}{e^{240/T_d} - 1} \quad (3)$$

The value of β depends on dust grain properties like composition, size, and compactness. For reference, a pure blackbody would have β = 0, the amorphous layer-lattice matter has β ∼ 1, and the metals and crystalline dielectrics have β ∼ 2.

For a smaller value of T_d, 1 can be dropped from both numerator and denominator of Eq. (3) and it takes the form

$$R = 0.6^{-(3+\beta)} \frac{e^{144/T_d}}{e^{240/T_d}} \quad (4)$$

Taking natural logarithm on both sides of Eq. (4) , we find the expression for the temperature as

$$T_d = \frac{-96}{\ln\{R \times 0.6^{(3+\beta)}\}} \quad (5)$$

where R is given by

$$R = \frac{F(60\mu m)}{F(100\mu m)} \quad (6)$$

F(60 μm) and F(100 μm) are the flux densities in 60 μm and 100 μm respectively. One can use Eq. (5) for the determination of the dust grain temperature.

DUST MASS ESTIMATION

Further analysis of the structure needs the mass of the structure. Dust masses are estimated from the infrared background corrected flux densities at 100 μm image. The distance of the structure was provided by Weinberger (2014). We are calculating dust mass following the analysis of Meaburn *et al.* (2000). The infrared flux can be measured from IRAS Sky View images and images from the Groningen using ALADIN2.5. The resulting dust mass depends on the physical and chemical properties of the dust grains, the adopted dust temperature and the distance to the object. The final expression for the dust mass can be written as:

$$M_{dust} = \frac{4\rho\rho}{3Q_n} \left| \frac{S_n D^2}{B(\nu, T)} \right| \quad (7)$$

where, a = weighted grain size , ρ = grain density, Q_ν = grain emissivity

$S_\nu = f \times MJy/Str \times 5.288 \times 10^{-9}$ where, 1 MJy/Str = 1×10^{-20} Kg s^{-2} and f = relative flux density measured from the image (IRAS 100 μm image).

D = distance of the structure

B(ν, T) = Planck's function, which is the function of the temperature and the frequency and given by the expression:

$$B(\nu, T) = \frac{2h\nu^3}{C^2} \left[\frac{2hc}{e^{\frac{h\nu}{kT}} - 1} \right] \quad (8)$$

where, h = Planck's constant, c = velocity of light

ν = frequency at which the emission is observed, T = the average temperature of the region

Value of various parameters we use in the calculation of the dust mass in our region of interest are as follows:

a = 0.1 μm (Young *et al.*, 1993)

ρ = 1000 Kg m^{-3} (Young *et al*., 1993)

Qν = 0.0010 for 100 μm and 0.0046 for 60 μm respectively (Young *et al*., 1993).

Using these values the expression (7) takes the form:

$$M_{dust} = 0.4 \left[\frac{S\nu D^2}{B(\nu, T)} \right] \quad (9)$$

We use the above equation for the calculation of the dust mass.

RESULTS AND DISCUSSION

Structure: Contour Maps

While going through the systematic search we discovered an isolated cavity in the spectrum of the 100 μm and 60 μm at the R.A. 04h 15m 03s and DEC 54° 41 m 00 s. With the help of the software ALADIN2.5, we have drawn the contour maps to distinguish the minimum flux region in the field of the interest. We select the contour level at 40 and major axis, minor axis and line passing through minimum temperature and minimum flux was drawn which was shown in the Fig 4. While drawing the major axis and the minor axis we should pass it through the minimum flux pixel.

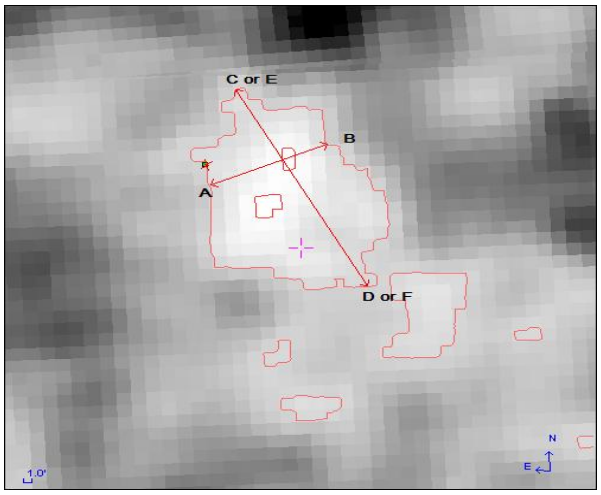

Fig. 4. The image of IRAS survey of the R.A. 04h 15m 03s and DEC 54◦ 41 m 00 s at the contour level 1-40 with major axis AB, minor axis CD, line joining minimum temperature and minimum flux EF.

This gives the distance of major diameter of the structure is 1.93 pc and minor diameter of the structure is 0.89 pc, whose calculation is shown latter.

FLUX DENSITY VARIATION

By using the ALADIN 2.5 software, flux density variation of the region of interest is studied. We obtained the graph of flux density variation along the major axis, minor axis and line joining the minimum temperature region and minimum flux region considering R.A. 04h 15m 03 s and DEC 54◦ 41m 00 s as center. We plotted it with the help of the ORIGIN5.0 for the polynomial fit of the data as in figure 5(a).

The polynomial equation of the fitted line is,

S_v =36.21 -25.77d +113.47 d^2-220.70 d^3+197.45 d^4-81.32 d^5 +12.57 d^6

Similarly the variation of flux density along minor diameter is plotted as in figure 5(b).

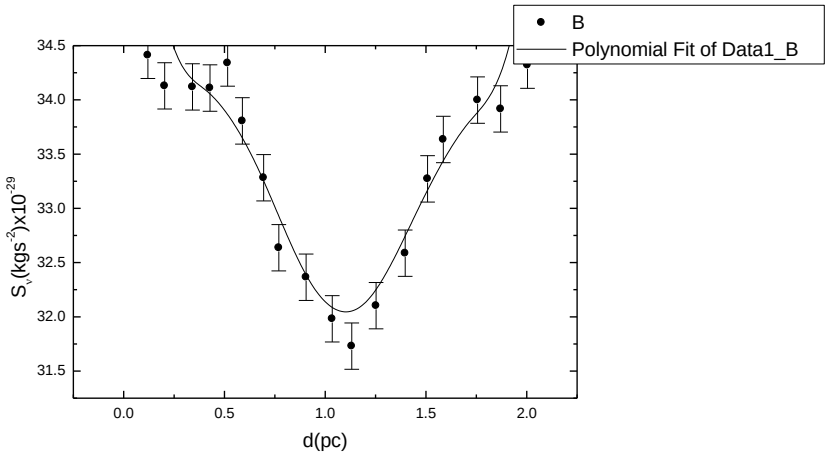

(a)

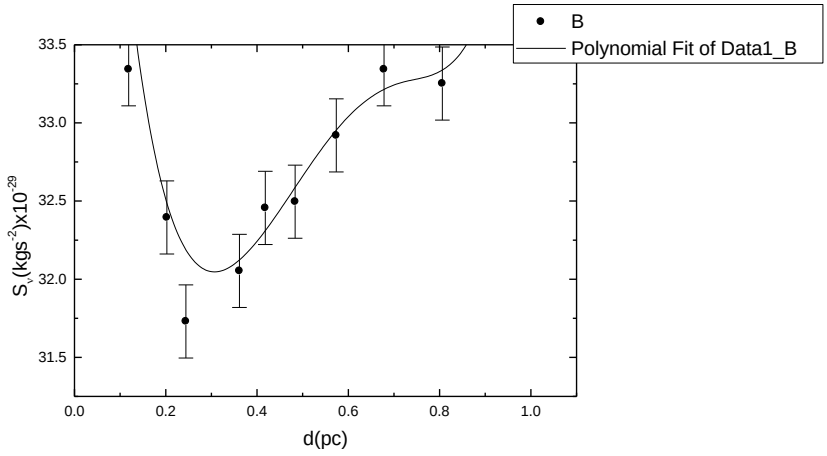

(b)

Fig. 5. Best fit polynomial showing the variation of flux density along (a) major diameter and (b) minor diameter of isocontour level 1-40. The distribution of flux density along major and minor diameters with distance of AGB star AGB 04153, +5441 and standard error of the distribution $\pm\sigma/\sqrt{n}$.

The polynomial equation of the fitted line is,

S_v=38.21-65.39d+265.19d^2-574.09d^3+777.16d^4-615.19d^5+209.22d^6

Then we studied the variation of flux density with the distance along the line joining the minimum flux and minimum temperature. But in this case major diameter and line joining between minimum flux and minimum temperature coincides.

DUST COLOR TEMPERATURE VARIATION

Using the method of Schnee *et al.* (2005), we calculated dust color temperature of each pixel inside the outer isocontour 40 in the region of interest. We use the IRAS 100 μm and 60 μm FITS images downloaded from the IRAS server (Web, 2014). For the calculation of temperature we choose the value of β = 2 following the explanation given by Dupac *et al.* (2003). The region with minimum and maximum temperature is found to lie in the range of 20.53 K to 21.09. So offset temperature is 0.56 K. It means for low temperature variation, there is symmetric outflow or symmetric distribution of density and temperature. Variation of temperature along major diameter AB with distance is shown in figure 7.

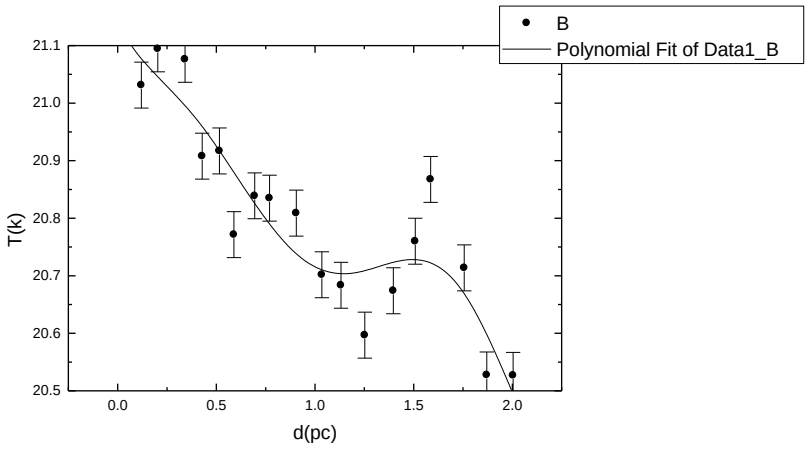

Fig. 7. Showing the variation of dust temperature with distance along major diameter AB of isocontour level 1-40 of the same AGB star. The solid circle with $\pm\sigma/\sqrt{n}$ error bar represents the standard error of the distribution. The solid curve represents the best fit polynomial (6th order polynomial).

The polynomial equation of the fitted line is,

T=21.10-0.41d+1.64d^2-5.42d^3+6.20d^4-2.87d^5+0.46d^6

Variation of dust temperature along minor diameter CD with distance is shown in figure 8.

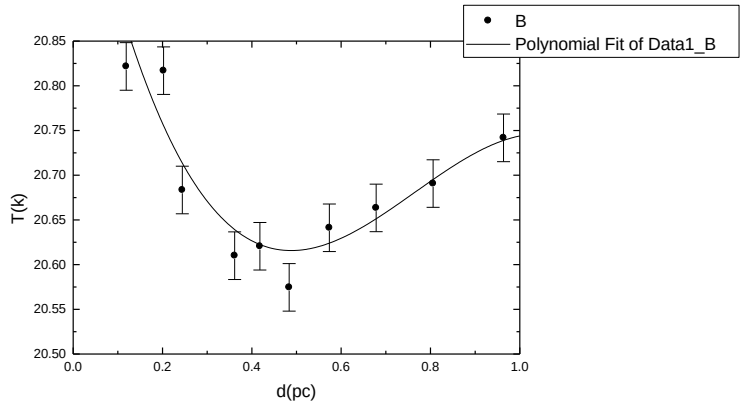

Fig. 8. Showing the variation of dust temperature with distance along minor diameter CD of isocontour level 1-40 of the same AGB star. The solid circle with $\pm\sigma/\sqrt{n}$ error bar represents the standard error of the distribution. The solid curve represents the best fit polynomial (3rd order polynomial).

The polynomial equation of the fitted line is,
$T=21.08- 2.32d+ 3.52d^2- 1.53d^3$.

Similarly major diameter and line joining between minimum temperature and minimum flux is same so the variation of dust temperature along line joining between minimum temperature and minimum flux EF with distance is already shown in figure 7.

The region in which minimum and maximum temperature is found in the range of 20.53K to 21.09 K with an offset temperature of dust 0.56 K . Such low offset temperature variation shows that there is symmetric outflow or symmetric distribution of density and temperature. It further suggests that our structure is not independently evolved or the role of discrete point sources in the field of cavity is important for the structure destruction mechanism. The cavity may be in thermally pulsating phase. The dust color temperature less than 20 K represents the interstellar cirrus cloud. Thus our far infrared dust structure (i.e. Cavity) is not a cirrus cloud. Another region of cloud fulfill the criteria of Cirrus clod.

SIZE OF THE STRUCTURE

To measure the major and minor diameter for each FITS image, we used a simple expression for the calculation, $L = R \times \theta$, where R = 240pc is the distance of the structure from us provided by Weinberger (5) and θ = pixel size (in radian). After calculation the major and minor diameter of the cavity region are 1.93 pc and 0.89 pc respectively at contour level 40 in the 100 μm image. Thus, the size of the structure is 1.93 pc × 0.89 pc .

DUST MASS ESTIMATION

For the calculation of dust mass, we need the distance to the region of interest. The distance of the structure provided by Weinberger (2014) is 240 pc. By using the temperature of each pixel and corresponding distance of the structure, we calculated mass of each pixel. Average mass of each pixel is $1.006x10^{26}$ kg and total mass of the structure is $1.438x10^{28}$ kg.

CALCULATION OF EXCESS MASS

For calculation of excess mass, we have drawn two circles i.e. inner and outer circle with the help of software Aladin v8.0. Circle through major diameter is supposed as outer circle and the circle through minor diameter is supposed as inner diameter of the interested region. With the help of those circles we have calculated excess mass

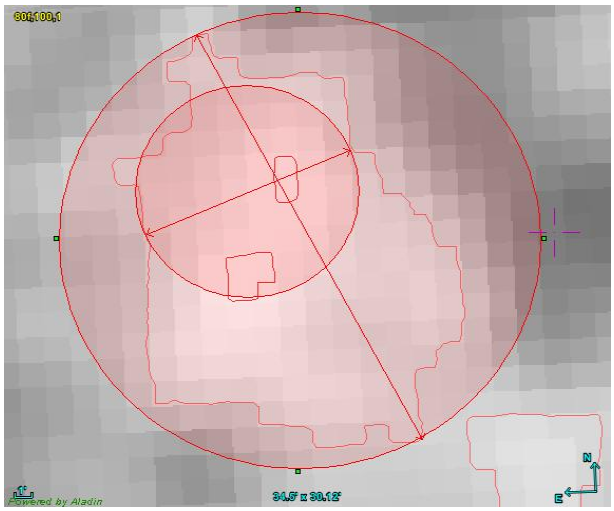

Fig. 9. Showing the inner circle and outer circle drawn in the structure for calculation of excess mass.

From the calculation total mass of the inner circle was found to be $6.054x10^{27}$ kg and average mass of inner circle was $1.009x10^{26}$ kg. Similarly the total mass of outer circle including inner circle was $2.699x\ 10^{28}$ kg and the average mass was $1.03x\ 10^{26}$ kg. So the total mass deficit in the inner pixel which was blown away by the AGB star is $2.094x\ 10^{28}$ kg i.e.o.0105 M_{sun}.

CONCLUSIONS

A systematic search of dust structure in the far infrared (100 μm and 60 μm) IRAS survey was performed using Sky View Virtual Observatory to find an isolated new cavity. We searched for the all C-rich AGB star surrounding in our galaxy, we found an isolated cavity like structure having cavity at both 60 μm and 100 μm wavelength at the center R.A. 04d 15m 03s and DEC 54◦ 41m 00s. The distance of the structure was found to be 240 pc[5]. The software ALADIN 2.5 is used for the data reduction and ORIGIN 5.0 for the plotting graphs. The physical properties of the structure, a study of flux density and temperature variation, dust color temperature, mass of dust, mass deficit per pixel of the cavity was calculated. The conclusions drawn from the present calculations are as follows:

- The major and minor diameter of the cavity like structure is found to be 1.93 pc and 0.89 pc respectively.

- The maximum and minimum flux was found to be at R.A. 04h 14m 14.9s DEC +54◦ 37m 01s & R.A. 04h 15m 10.9s DEC +54◦ 51m 08s, maximum and minimum temperature is at R.A. 04h 14m 25.2s DEC +54◦ 38m 03s & at R.A. 04h 15m 46.1s DEC +55◦ 00m 07s respectively.
- The region in which minimum and maximum temperature is found in the range of 20.53K to 21.09 K with an offset temperature of dust 0.56 K which shows that the cavity is independently evolved. Such low offset temperature variation shows that there is symmetric outflow or symmetric distribution of density and temperature.
- The total mass of the inner circled cavity was 6.054×10^{27} Kg, the average mass of the inner circle was 1.009×10^{26} Kg and that of the outer circle including inner was 2.699×10^{28} Kg and 1.03×10^{26} Kg respectively. The total mass deficit of the structure was 2.094×10^{28} Kg i.e. 0.0105 M_{sun}.

REFERENCES

Aryal B., and Weinberger R. (2006). A & A **446**:213.

Aryal B.; Rajbahak C., and Weinberger R. (2010). MNRAS **402**:1307.

Dupac X.; Bernard J. P.; Boudet N.; Giard M.; Lamarre J. M.; Meny C. *et al.* (2003). A & A **404**.

Herwig F. (2005). A & A **43**:435.

Hollowell, D., and Iben, I. (1988). Jr. APJL, **333**:25.

Lagadec E.; Mekarnia D.; de Freitas Pacheco J. A., and Dougados C. (2005). A & A **433**:553.

Marigo P. and Girardi L. (2007). A & A **469**:239.

Meaburn J.; Redman M. P.; Connor O.; Holloway A. J., and Bryce M. (2000). MNRAS **312**:23.

Reimers D. (1975). Problems in Stellar Atmospheres and Envelopes, eds. Bascheck, B.; Kegel W. H., and Traving, G. (springer: Berlin), p.229

Renzini A., and Fusi Pecci F. (1988). ARA & A **26**:199.

Schnee S. L. (2006). Gas and Dust in the Molecular Cloud: Density, Temperature and Velocity Structure, Ph.D. Thesis, Harward University, Cambridge Massachusetts.

Schnee, S. L.; Ridge N. A.; Goodman A. A., and Jason G. L. (2005). APJ, **634:**442.

Schroder K. P., and Cuntz M. (1993). APJL **630**:73.

Suh K. W., and Kwon Y. J. (2011). MNRAS **417**: 3047.

Vassiliadis E., and Wood P. R. (1993). APJ **413**:641.

Web (2014). http://skyview.gsfc.nasa.gov/current/cgi/query.pl

Weinberger R. (2014). Private Communication.

Wood P. R. (2010). SAIt **81**:883.

Young K.; Phillips T. G., and Knapp G. R. (1993). APJ **409**:725.